toxins

MDPI

Article

# Newly Discovered Action of HpTx3 from Venom of *Heteropoda venatoria* on Nav1.7 and Its Pharmacological Implications in Analgesia

**Xinzhou Wu, Zhouquan Wang, Yu Chen, Dehong Xu, Peng Zhang and Xianchun Wang ***

Key Laboratory of Protein Chemistry and Developmental Biology of Ministry of Education, College of Life Sciences, Hunan Normal University, Changsha 410081, China; wuxinzhouwu@163.com (X.W.); wangzhouquan123@sina.com (Z.W.); chenyu525788@163.com (Y.C.); xudehong163@126.com (D.X.); zhangpeng19912019@163.com (P.Z.)

* Correspondence: wang_xianchun@263.net

Received: 4 October, 2019; Accepted: 18 November 2019; Published: 20 November 2019

**Abstract:** It has been reported that Heteropodatoxin3 (HpTx3), a peptidic neurotoxin purified from the venom of the spider species *Heteropoda venatoria*, could inhibit $K_v$4.2 channels. Our present study newly found that HpTx3 also has potent and selective inhibitory action on $Na_v$1.7, with an $IC_{50}$ of 135.61 ± 12.98 nM. Without effect on the current–voltage (I-V) relationship of $Na_v$1.7, HpTx3 made minor alternation in the voltage-dependence of activation and steady-state inactivation of $Na_v$1.7 (4.15 mV and 7.29 mV, respectively) by interacting with the extracellular S3–S4 loop (S3b–S4 sequence) in domain II and the domain IV of the $Na_v$ channel subtype, showing the characteristics of both pore blocker and gate modifier toxin. During the interaction of HpTx3 with the S3b–S4 sequence of $Na_v$1.7, the amino acid residue D in the sequence played a key role. When administered intraperitoneally or intramuscularly, HpTx3 displayed potent analgesic activity in a dose-dependent manner in different mouse pain models induced by formalin, acetic acid, complete Freund's adjuvant, hot plate, or spared nerve injury, demonstrating that acute, inflammatory, and neuropathic pains were all effectively inhibited by the toxin. In most cases HpTx3 at doses of ≥ 1mg/kg could produce the analgesic effect comparable to that of 1 mg/kg morphine. These results suggest that HpTx3 not only can be used as a molecular probe to investigate ion channel function and pain mechanism, but also has potential in the development of the drugs that treat the $Na_v$1.7 channel-related pain.

**Keywords:** HpTx3; $Na_v$1.7; inhibition; selectivity; analgesia; mouse pain model; *Heteropoda venatoria*

**Key Contribution:** The HpTx3 from the venom of spider *Heteropoda venatoria* was for the first time found to have potent and selective inhibitory action on $Na_v$1.7. Its action mechanism and pharmacological implications in analgesia were systematically investigated, which not only accumulated new data for the investigation of ion channel function and pain mechanism, but also provided a new lead molecule for the development of the drugs to treat $Na_v$1.7-related pain.

## 1. Introduction

The voltage-gated sodium channel ($Na_v$) in mammalian cells is a multiple transmembrane protein that can be activated by voltage and then permits the $Na^+$ to enter the cell. To date, a total of nine kinds of $Na_v$ subtypes have been found and named $Na_v$1.1–1.9 [1,2]. A $Na_v$ channel consists of a pore-forming $\alpha$ subunit and one or two $\beta$ subunits and only the $\alpha$ subunit is required for function. The $\alpha$ subunit is composed of four homologous domains. Each domain contains six transmembrane

helices (S1–S6) and a certain number of extra- and intra-cellular loops connect these transmembrane helices. S1–S4 have been shown to sense voltage and S5–S6 to construct the central pore [3]. Although the $Na_v$ channel has diverse in vivo distribution profiles and biological functions, its fundamental function is to produce and transmit currents in cell membrane by permitting the flow of ions [4]. The disorder of a $Na_v$ channel often leads to many kinds of diseases, collectively named ion-channel diseases. For example, $Na_v1.7$ dysfunction is closely involved in pain [5]. Pain is a protective sensation that serves to warn us of impending harm and makes us withdraw from and subsequently avoid injurious situations. However, abnormal pain will deteriorate patients' life quality, expend medical resources, or even threat patients' lives. $Na_v1.7$ is primarily expressed in the peripheral nervous system and participates in the linkage of stimuli and pain signaling pathway. Sensory neurons in the peripheral nervous system can produce action potential when the stimulation is applied, and $Na_v1.7$ plays an important role in initiating such action potentials [5,6]. It has been well-established that $Na_v1.7$ is highly expressed in dorsal root ganglia neurons and its mutations induce genetic pain and painless disorders, which makes $Na_v1.7$ one of the most promising targets for pain control [7–9]. For example, gain-of-function mutation in the *SCN9A* gene that encodes the $\alpha$ subunit of $Na_v1.7$ caused severe episodic pain, whereas loss-of-function mutations in *SCN9A* resulted in insensitivity to pain [10]. Furthermore, many reports indicate that the gating modulators and pore blockers of $Na_v1.7$ can affect the sensitivity of a patient to pain [11]. Therefore, the agents targeting $Na_v1.7$ can help patient relief or treat the $Na_v1.7$-related pain syndromes [5].

Up to date, a batch of small molecules that target $Na_v$ channels are well established to attenuate the pain in humans, such as opioids [12] and tetrodotoxin (TTX), a well-known blocker of $Na_v$ channels [13]. Nevertheless, due to their intrinsic limitations, such as lack of specificity and/or pronounced side-effects, the potential of these small molecules in the therapeutic development is significantly weakened, which promotes development of the drugs with higher efficiency and less side effects from natural resources. In recent decades, the proteinaceous toxins with an analgesic effect from the venomous spiders have attracted the attention of the relevant scientific researchers [7,14]. Spider venom produced by venom glands can help spiders resist the natural enemies and capture preys. The venom is a highly complex mixture composed of small molecules, peptides, proteins, etc. Peptides are often of high level in the spider venom and many of them can specifically act on ion channels, including $Na_v1.7$ [15,16], and thus have potential in the development of drugs that treat $Na_v$ 1.7 subtype-related diseases.

In this paper, we isolated a peptide toxin, named Heteropodatoxin3 (HpTx3) [17], from the venom of the spider *Heteropoda venatoria* and proved that HpTx3 has high potency and selectivity against $Na_v1.7$. Using multiple rodent pain models, HpTx3 was demonstrated to have a powerful analgesic effect.

## 2. Results

### *2.1. Preparation and Identification of HpTx3*

After the venom was electrically collected from the spider species *Heteropoda venatoria* and was subjected to semipreparative RP-HPLC, it was separated into more than ten primary chromatographic peaks (Figure 1). The peak marked with an asterisk corresponded to that containing HpTx3 in the RP-HPLC chromatogram of the *Heteropoda venatoria* venom reported by Sanguinetti et al. [17], and was collected and further purified with an analytical C18 column, which gave a single symmetric peak (inset in Figure 1), suggesting that the sample was purified to homogeneity. The mass spectrometric analysis indicated that the venom component existed primarily in the form of multiple-charge ions with 2, 3, 4, and 5 positive charges, respectively (Figure 2). From the *m*/*z* values of its ion peaks, the monoisotopic molecular weight of the component was calculated to be 3596.46 (average molecular weight 3599), which was consistent with the theoretical monoisotopic molecular weight of the Heteropodatoxin3 (HpTx3) with an amide on its C-terminal [17]. In view of the fact that the acquired venom component and the reported HpTx3 had the corresponding peak position in RP-

HPLC chromatogram and the same molecular weight, the component we purified from the *Heteropoda venatoria* venom was identified as peptide neurotoxin HpTx3.

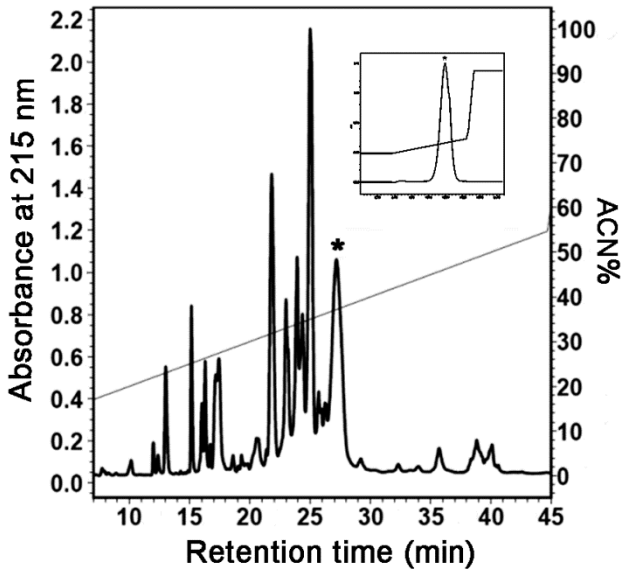


**Figure 1.** RP-HPLC chromatograms of the *Heteropoda venatoria* venom. The asterisk (*) indicates the peak of interest and the inset shows its further purification by analytical RP-HPLC.

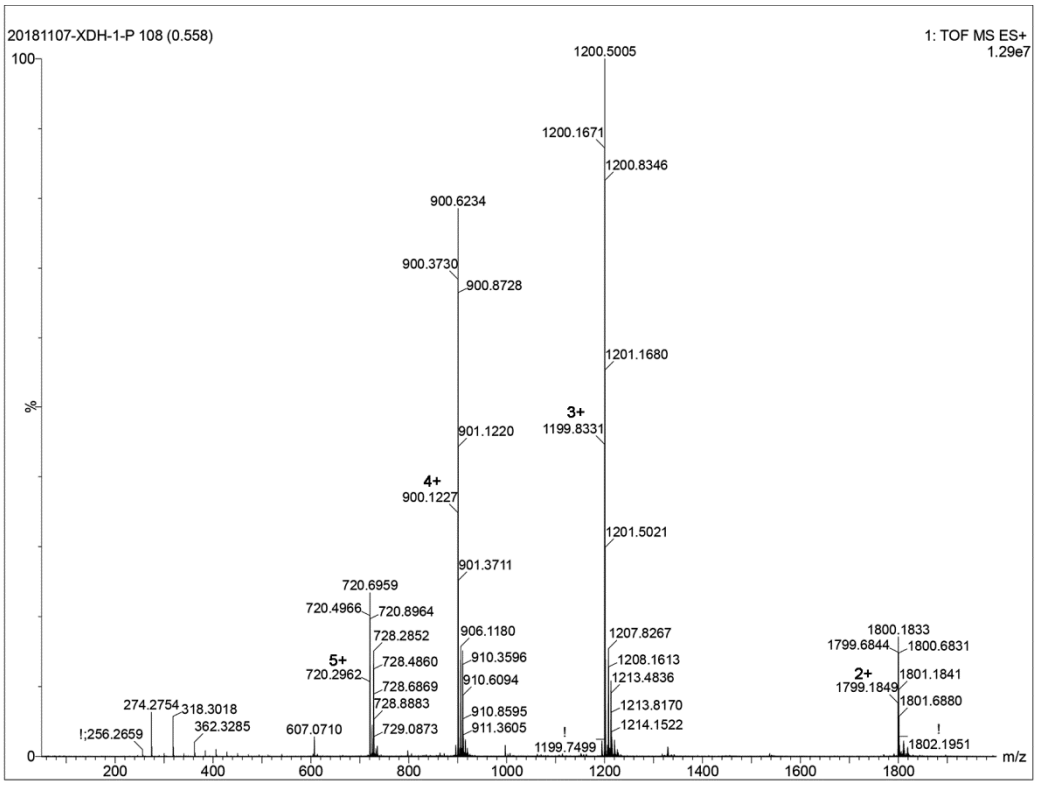


**Figure 2.** Determination of the molecular weight of Heteropodatoxin3 (HpTx3) by mass spectrometry.

## 2.2. Effects of HpTx3 on $Na_v$ Channel Subtypes

By sequence alignment, we found that the sequence of HpTx3 has high identity with those of some $Na_v$ channel peptide toxins in the NaSpTx family 3 [7,18] (see Discussion), which suggested

that HpTx3 might have an inhibitory effect on $Na_v$ channels. In order to investigate the $Na_v$ channel-targeted activity and the subtype selectivity of HpTx3, the effects of HpTx3 on mammal $Na_v1.2$–1.9 expressed in HEK293T or ND7/23 cells were detected. The results demonstrated that 1 μM HpTx3 inhibited the $Na_v1.7$ currents completely, $Na_v1.6$ currents by 46.0%, and $Na_v1.5$ currents by 12.8%, without effects on $Na_v1.2$, $Na_v1.3$, and $Na_v1.4$; even 10 μM HpTx3 did not affect the currents of $Na_v1.8$ and $Na_v1.9$ (Figure 3A–H). Comparatively, HpTx3 most potently inhibited $Na_v1.7$ ($IC_{50}$ 135.61 ± 12.98 nM), with 145-fold selectivity over $Na_v1.2$ ($IC_{50}$ 19.71 ± 0.49 μM), 104-fold selectivity over $Na_v1.3$ ($IC_{50}$ 14.11 ± 2.5 μM), 136-fold selectivity over $Na_v1.4$ ($IC_{50}$ 18.5 ± 0.21 μM),-122-fold selectivity over $Na_v1.5$ ($IC_{50}$ 16.51 ± 0.85 μM), 7-fold selectivity over Nav1.6 ($IC_{50}$ 972.10 ± 1.50 nM), and even greater selectivity over $Na_v1.8$ and $Na_v1.9$ whose $IC_{50}$ values were not determined in view of the fact that 10 μM HpTx3 did not significantly affect their currents. These data demonstrated that the effect of HpTx3 on $Na_v$ channels has obvious subtype selectivity (Figure 3I).

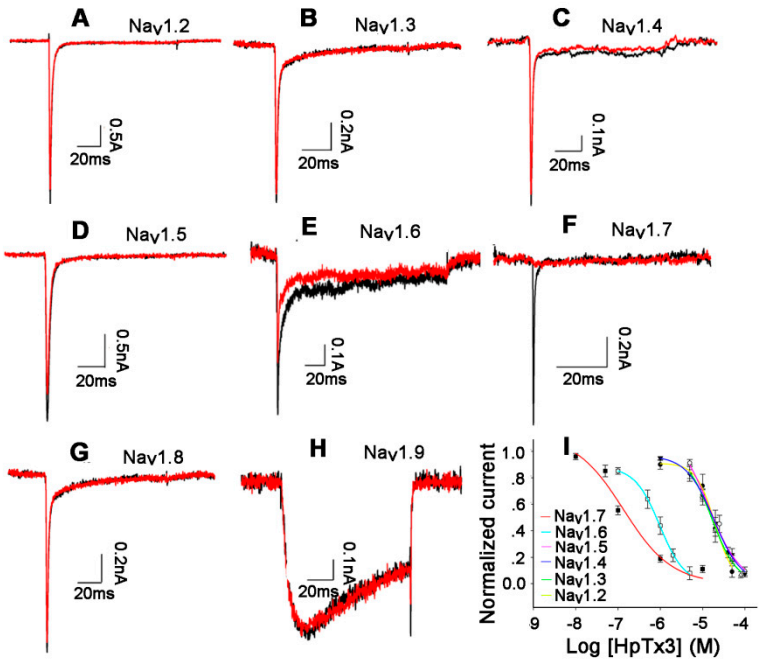


**Figure 3.** Effects of HpTx3 on $Na_v$ channel subtypes. (**A–H**) Representative current traces of $Na_v$ subtypes ($Na_v1.2$–1.9, respectively) before (black) and after (red) addition of 1 μM ($Na_v1.2$–1.7) or 10 μM ($Na_v1.8$–1.9) HpTx3 (n = 4–6); (**I**) concentration-response curves for the inhibition of $Na_v$ subtypes by HpTx3 (n = 4–6).

### *2.3. Effects of HpTx3 on the Voltage-Dependence of $Na_v1.7$ Activation and Inactivation*

When the current–voltage (I–V) relationship for $Na_v1.7$ affected by HpTx3 was investigated, the results indicated that HpTx3 (0.20 μM) voltage-dependently decreased the currents of $Na_v1.7$ at the voltages ranging from –40 mV to + 70 mV, but did not significantly alter the threshold value of initial activation voltage (–40 mV), the maximum activation voltage (+10 mV) and the reversal voltage (+70 mV) of the $Na_v$ channel subtype (Figure 4A), suggesting that the application of the toxin did not change the ion selectivity of $Na_v1.7$ channel in the tested depolarizing voltages. However, as shown in Figure 4B, compared with the control, HpTx3 (0.25 μM) shifted the steady-state activation curve of $Na_v1.7$ to the right (more depolarized membrane voltage) by about 4.15 mV, with half-activation voltages before and after the application of HpTx3 being –14.20 ± 1.27 mV and –10.05 ± 0.96 mV, respectively. The analysis of inactivation kinetics of the $Na_v1.7$ showed that the half-inactivation voltages before and after the application of 0.25 μM HpTx3 were –68.71 ± 0.58 mV and –76 ± 0.78 mV, respectively, shifting the steady-state inactivation curve to the left (more polarized membrane voltage) by 7.29 mV (Figure 4C), indicating that HpTx3 facilitated the steady-state inactivation of the $Na_v1.7$ channel subtype to a certain degree.

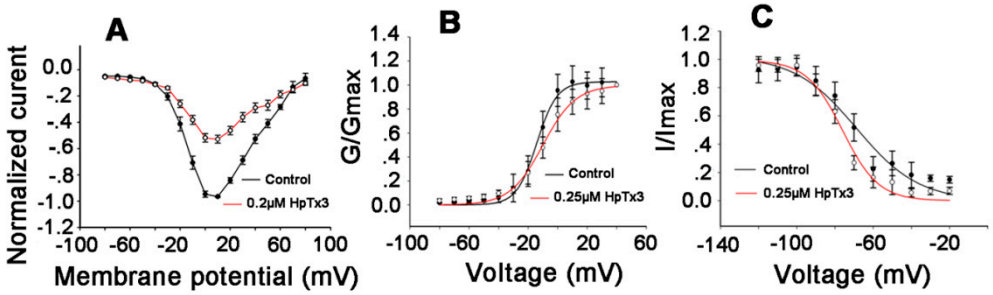


**Figure 4.** Effects of HpTx3 on the voltage-dependence of $Na_v1.7$ activation and steady-state inactivation. **(A)** Current–voltage (I-V) curve for $Na_v1.7$ before (black) and after (red) application of HpTx3 (n = 6); **(B)** steady-state activation curves of $Na_v1.7$ before (black) and after (red) application of HpTx3 (n = 6); **(C)** steady-state inactivation curves of $Na_v1.7$ before (black) and after (red) application of HpTx3 (n = 6). Data are shown as mean ± SD.

### *2.4. Action Sites of HpTx3 on $Na_v1.7$*

In order to identify the action sites of HpTx3 on $Na_v1.7$, we inserted DIIS3b–S4, DIII, and DIV sequences of $Na_v1.8$, on which 10 μM HpTx3 had no inhibitory effect (Figure 3G), into the $Na_v1.7$ to replace the counterpart sequences and thus prepared three chimeras named $Na_v1.7$/1.8DIIS3b–S4, $Na_v1.7$/1.8DIII, and $Na_v1.7$/1.8DIV, respectively (Figure 5A–E), followed by patch clamp analysis to detect the effects of HpTx3 on the currents of the resulting chimeras expressed in HEK293T cells. The analytical results indicated that 1 μM HpTx3 showed no significant effects on the currents of $Na_v1.7$/1.8DIV (Figure 5D) and $Na_v1.7$/1.8DIIS3b–S4 (Figure 5E), and the current of the $Na_v1.7$/1.8DIII was enhanced by the toxin at the same concentration (Figure 5C). These results demonstrated that the DIV and DIIS3b–S4, an extracellular loop of DII, of the $Na_v1.7$ are involved in the interaction between HpTx3 and $Na_v1.7$; the mechanism of action of HpTx3 was speculated to be at least partially similar to that of site 4 toxins that use DIIS3b–S4 as a key action site [19,20]. In order to further identify the key residues in the DIIS3b–S4 sequence of $Na_v1.7$, we first compared the DIIS3b–S4 sequences of $Na_v1$ subtypes (Figure 5F). As shown in Figure 5F, the D/E and E/Q may be the amino acids of potential binding sites. We focused on comparing the S3b–S4 sequence of $Na_v1.7$ with that of $Na_v1.4$, on which 1 μM HpTx3 showed no inhibitory effect (Figure 3C), and found that only two amino acid residues are different: D in $Na_v1.7$ DIIS3b–S4 compared to N in $Na_v1.4$ DIIS3b–S4 and E in $Na_v1.7$ DIIS3b–S4 compared to Q in $Na_v1.4$ DIIS3b–S4. Therefore, we mutated the two acidic amino acid residues of $Na_v1.7$ DIIS3b–S4 into neutral ones, D into N ($Na_v1.7$ D816N) and E into Q ($Na_v1.7$ E818Q). Patch clamp analysis showed that 1 μM HpTx3, which could inhibit the current of wild type $Na_v1.7$ completely (Figure 3F), inhibited the current of $Na_v1.7$ D816N by only 23.7% (Figure 5G), with an $IC_{50}$ value of 3.13 ± 2.6 μM, compared to 135.61 ± 12.98 nM for wild type $Na_v1.7$ (Figure 5I), showing a 23-fold difference. On the contrary, 1 μM HpTx3 inhibited the current of the $Na_v1.7$ E818Q by about 80% (Figure 5H). These data demonstrated that, during the HpTx3 interaction with $Na_v1.7$, residue D816 in the DIIS3b–S4 sequence of $Na_v1.7$ plays a crucial role, and E818 only plays a minor role.

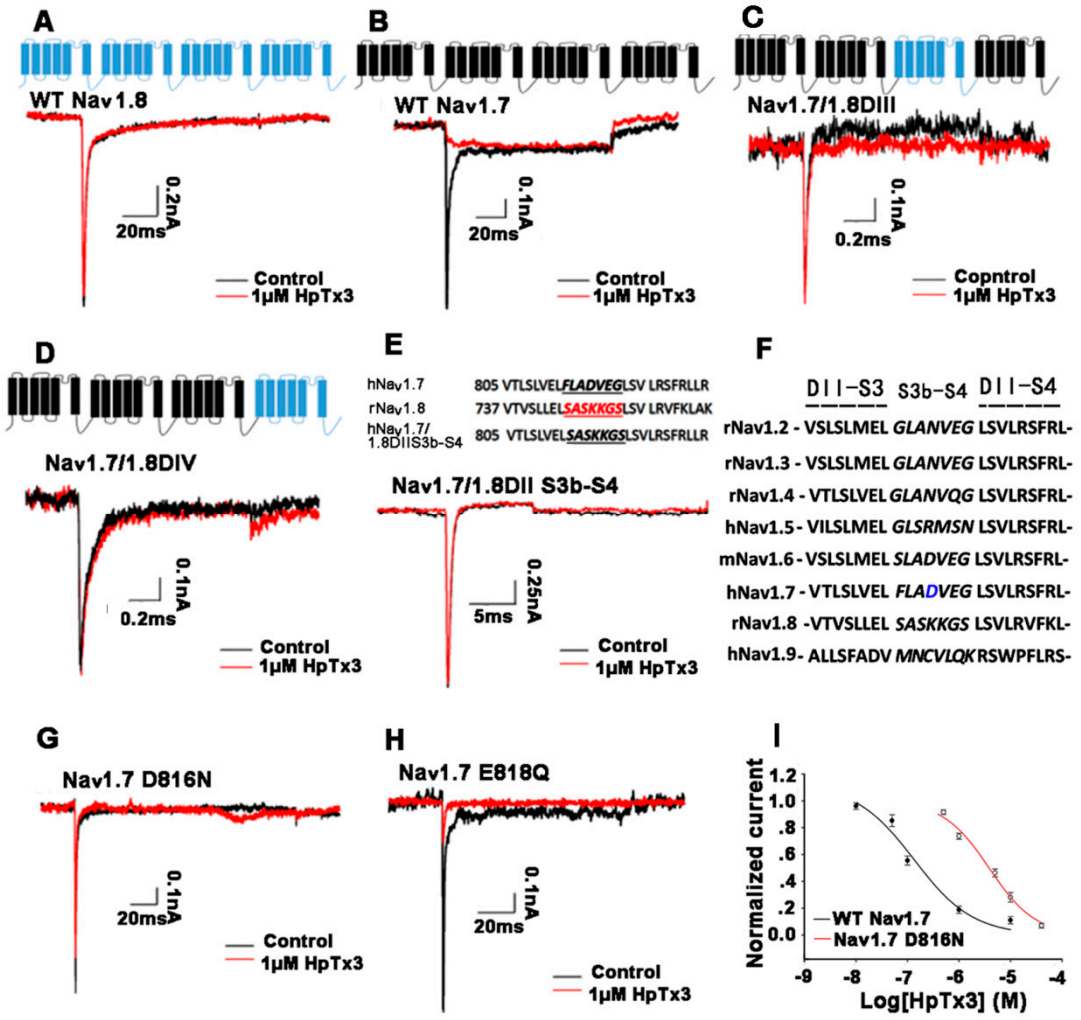


**Figure 5.** Effects of HpTx3 on the currents of chimeras and single mutants. (**A, B**) Membrane topology of wild type Na$_v$1.7 and Na$_v$1.8, and the effect of HpTx3 on their currents; (**C, D**) membrane topology of chimeras Na$_v$1.7/1.8DIII and Na$_v$1.7/1.8DIV, and the effect of HpTx3 on their currents; (**E**) construction of Na$_v$1.7/1.8DIIS3b–S4 and the effect of HpTx3 on its current; (**F**) alignment of the S3b–S4 sequences of Na$_v$ subtypes. The key amino acid residue is highlighted with blue color; (**G, H**) effect of HpTx3 on the currents of Na$_v$1.7 D816N and Na$_v$1.7 E818Q; (**I**) concentration-response curves of HpTx3 on wild type Na$_v$1.7 and Na$_v$1.7 D816N. n = 6.

### *2.5. Analgesic Effects of HpTx3 in Mouse Pain Models*

In order to probe into the pharmacological implications of HpTx3 in analgesia, we used different mouse pain models, including those induced by formalin, acetic acid, complete Freund's adjuvant, hot plate, and spared nerve injury, to detect the effects of the toxin on the pain-like behaviors of the mice. The pain models could be classified into acute inflammation models induced by formalin and acetic acid, chronic inflammation pain model induced by complete Freund's adjuvant, acute thermal pain model induced by hot plate, and chronic neuropathic pain model induced by spared nerve injury.

#### 2.5.1. Formalin Model Test

In the formalin-induced mouse pain model, nociceptive behaviors such as paw-licking, swinging legs, and retractable legs in mice were induced by-subcutaneous injection of formalin. The effect of HpTx3 on the formalin-induced nociceptive behaviors was assessed by comparing the times

in seconds of paw licking in mice injected intramuscular with 100 μL 0.9% saline (control), morphine (1 mg/kg, positive control), or HpTx3 (0.2, 1, and 5 mg/kg). Paw licking times were tallied in 5-min time bins over 35 min following formalin injection (Figure 6). As shown in Figure 6A, the nociceptive reaction included phase I (0–10 min after formalin injection) and phase II (15–35 min after formalin injection), which were mainly caused by the direct activation of nociceptive neurons and the formalin-induced inflammation, respectively [21,22]. Compared with the control, HpTx3 shortened the paw licking times in both of the two phases, indicating that the toxin could attenuate the nociceptive behaviors caused by both nociceptive neuron activation and inflammation. In phase I, the total paw licking times of the mice in the control group were 248 s, while those of the mice in the groups treated with 0.2, 1, and 5 mg/kg HpTx3 were 106 s, 85.3 s, and 45.3 s, shortening the paw licking times by 57.26% ($p < 0.01$), 65.60% ($p < 0.01$), and 81.73% ($p < 0.001$), respectively (Figure 6B). In phase II, the total paw licking times of the mice in the control group were 572.7 s, while those of the mice in the groups treated with 0.2, 1, and 5 mg/kg HpTx3 were 424.3 s, 210.3 s, and 49 s, decreasing the times by 25.91% ($p < 0.05$), 63.27% ($p < 0.01$), and 91.44% ($p < 0.001$), respectively. These data demonstrated that HpTx3 at the tested concentrations could significantly attenuate the nociceptive behaviors induced by formalin and the analgesic effects of HpTx3 in both of the two phases were dose-dependent. In addition, the total paw licking times of the mice in the group treated with 1 mg/kg morphine were 99 s in phase I and 134.3 s in phase II, respectively. Comparison of the licking times showed that the paw licking times after injection of 0.2, 1 and 5 mg/kg HpTx3 in phase I, and 1 and 5 mg/kg HpTx3 in phase II were not significantly different from those after injection of 1 mg/kg morphine ($p > 0.05$), suggesting their comparable analgesic effects.

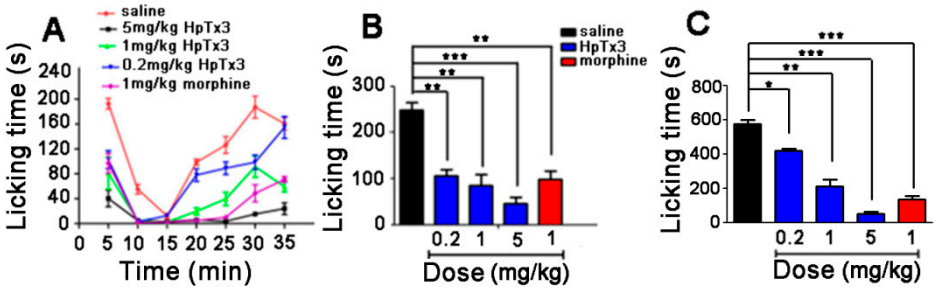


**Figure 6.** Effects of HpTx3 on the paw licking time of the mice in formalin-induce pain model. **(A)** Licking time at different time points after injection; **(B)** total licking time in phase I after injection; **(C)** total licking time in phase II after injection. The data are shown as mean ± SD, n = 8. * $p < 0.05$, ** $p < 0.01$, *** $p < 0.001$.

### 2.5.2. Acetic Acid-Induced Writhing Model Test

In the acetic acid-induced writhing model, the nociceptive behaviors were induced, including writhing, body stretching, abdomen sticking to the ground, etc. As shown in Figure 7, the average writhing number of the mice in the control group over 30 min was 40.3, while those of the mice in the test groups treated with HpTx3 at doses of 0.2, 1, and 5 mg/kg were 26.8, 17, and 10.8, decreasing the writhing number by 33.54% ($p < 0.05$), 57.76% ($p < 0.01$), and 73.29% ($p < 0.001$), respectively. These findings indicated that HpTx3 significantly decreased the number of abdominal writhing of the mice in a dose-dependent manner. The average abdominal writhing number of the mice intraperitoneally injected with morphine at a dose of 1 mg/kg was 16.8, compared to 17 for 1 mg/kg HpTx3 ($p > 0.05$) and 10.8 for 5 mg/kg HpTx3 ($p > 0.05$), respectively, demonstrating that in the acetic acid-induced writhing model 1 and 5 mg/kg HpTx3 produced analgesic action comparable to that of 1 mg/kg morphine ($p > 0.05$).

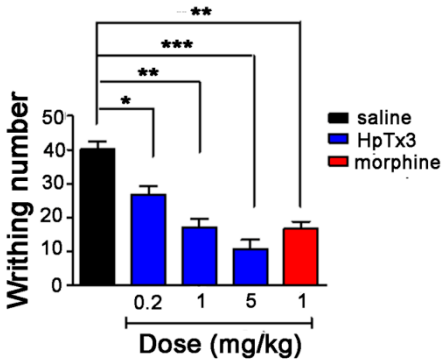


**Figure 7.** Effects of HpTx3 on the abdominal writhing number of the mice in acetic acid-induced writhing model. The data are shown as mean ± SD, n = 8. $^{*}p < 0.05$, $^{**}p < 0.01$, $^{***}p < 0.001$.

### 2.5.3. Complete Freund's Adjuvant (CFA) Model Test

Twenty-four hours after local inflammation in mice was induced by subcubaneous injection of complete Freund's adjuvant (CFA) into the plantar surface of the right hind paw, it led to nociceptive behaviors such as paw-licking and flinching. All the mice developed mechanical hyperalgesia in the inflamed hind paw, with an average withdrawal threshold of 0.70 ± 0.20 g compared to 1.85 ± 0.28 g before CFA injection. As shown in Figure 8A, intramuscular administration of 0.2, 1 and 5 mg/kg HpTx3 significantly increased the paw withdrawal thresholds to 0.94, 1 and 1.09 g, compared to 0.71 g of the control ($p < 0.001$), respectively, displaying an obvious dose-dependent analgesic effect. The strongest analgesic action of HpTx3 at the three different concentrations occurred at 1 h after HpTx3 injection. After this time point, the toxin still had a strong analgesic effect within the time range of the test, although having a decreasing tendency. Different from HpTx3, morphine, as a positive control in the present test, displayed the strongest analgesic effect at 0.5 h after injection, indicating that morphine exerted the analgesic action faster than HpTx3 in such a model. Figure 8B shows that HpTx3 increased the paw withdrawal threshold in a dose-dependent manner, and HpTx3 at all the used doses (0.2, 1, and 5 mg/kg) produced an analgesic effect close to that (paw withdrawal threshold 1.05 g) of 1 mg/kg morphine ($p > 0.05$).

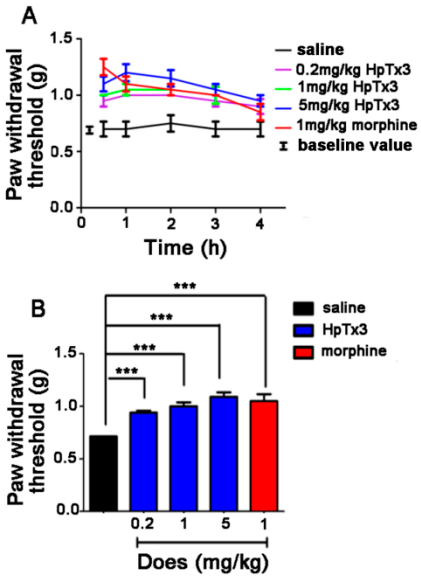


**Figure 8.** Effect of HpTx3 on the inflammatory pain-like behaviors in mice in complete Freund' s adjuvant (FCA) pain model. **(A)** Paw withdrawal threshold detected at different time points after FCA

injection; **(B)** comparison of average paw withdrawal threshold after injection with different concentrations of toxin or morphine. The data are shown as mean ± SD, n = 8. $^{***}p < 0.001$.

### 2.5.4. Hot Plate Pain Model Test

When the temperature of the hot plate was set at 55 ± 1 °C, the mice showed obvious nociceptive behaviors including paw-licking and paw lift. The paw withdrawal latency of the mice placed on the plate was determined in seconds at 0.5, 1.0, 1.5, and 2.0 h after injection. The paw withdrawal latency of the control (injection of 0.9% saline) remained relatively stable at all the time points, with an average paw withdrawal latency of 5.93 s. Intraperitoneal injection of HpTx3 increased the paw withdrawal latency at all four time points after injection, showing the most analgesic effect at 1.0 h (at doses of 1 and 5 mg/kg) as well as 0.5 h (at a dose of 0.2 mg/kg) (Figure 9A), while morphine displayed the most analgesic effect at 0.5 h after injection. The average paw withdrawal latency of the mice injected with HpTx3 at doses of 0.2, 1, and 5 mg/kg were 8.5, 10.07, and 11.7 s, which, compared with the control, increased paw withdrawal latency by 43.33% ($p < 0.01$), 69.81% ($p < 0.01$), and 97.3% ($p < 0.001$), respectively (Figure 9B). These results indicated that HpTx3 significantly raised the thermal pain threshold of the mice in a dose-dependent way. Furthermore, statistical analysis showed that the potency of 1 and 5 mg/kg HpTx3 to inhibit thermal pain-like behaviors was comparable to that (average paw withdrawal latency 11.03 s) of 1 mg/kg morphine ($p > 0.05$) (Figure 9B).

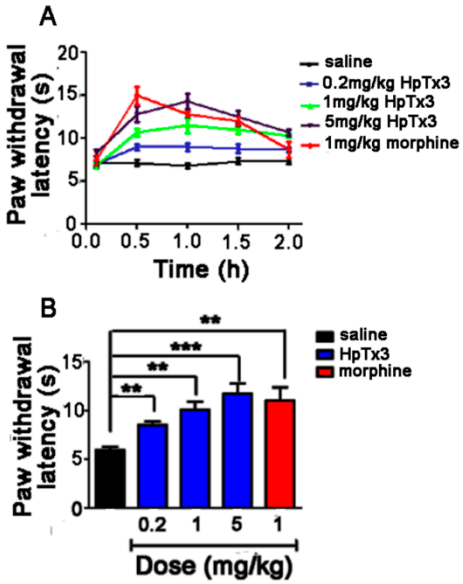


**Figure 9.** Effect of HpTx3 on paw withdrawal latency of the mice in hot plate pain model. **(A)** Paw withdrawal latency detected at different time points after injection; **(B)** Comparison of average paw withdrawal latency after injection with different concentrations of toxin or morphine. The data are shown as mean ± SD, n = 8. $^{**}p < 0.01$, $^{***}p < 0.001$.

### 2.5.5. Spared Nerve Injury (SNI) Model Test

Observation showed that, three days after the SNI surgery, the mice developed mechanical hyperalgesia that lasted for about one month at the ipsilateral paw, showing obvious nociceptive behaviors such as flinching and paw lift. We began to determine the paw withdrawal thresholds 18 days after the surgery. On the 18th day, the average paw withdrawal threshold in mice was 0.46 ± 0.10 g compared to 1.85 ± 0.28 g before the surgery, indicating that the SNI model was prepared successfully. As shown in Figure 10A, 1 and 5 mg/kg HpTx3 showed their highest analgesic activity at 0.5 h after injection, and 5 mg/kg HpTx3 produced stronger analgesic action than 1 mg/kg morphine at the time points after 3 h, indicating that 5 mg/kg HpTx3 could produce an analgesic

effect in an even longer time. The average paw withdrawal threshold of the mice in control was 0.47 g, and injection of 0.2, 1, and 5 mg/kg HpTx3 increased the average threshold to 0.71, 0.9, and 1 g, increased by 51.06%, 91.49%, and 112.77%, respectively ($p < 0.001$, Figure 10B). In addition, 1 mg/kg morphine led to an average paw withdrawal threshold of 1.05 g, showing a comparable analgesic effect to 1 and 5 mg/kg HpTx3 ($p > 0.05$).

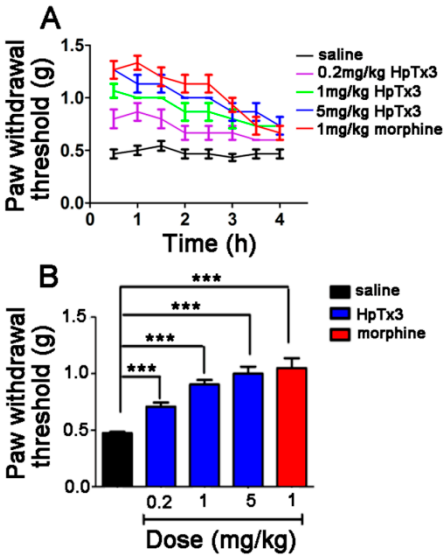


**Figure 10.** Effect of HpTx3 on paw withdrawal threshold of the mice following mechanical stimuli to the paw. The determination of paw withdrawal thresholds was made 18 days after the surgery. **(A)** Paw withdrawal thresholds detected at different time points after injection; **(B)** comparison of average paw withdrawal threshold after injection with different concentrations of toxin or morphine. The data are shown as mean ± SD, n = 8. $^{***}p < 0.001$.

### *2.6. In Vivo Toxicity and the Effect of HpTx3 on the hERG Channel*

For detecting the potential in vivo toxicity of HpTx3, we chose eight C57BL/6 mice and intraperitoneally injected each of them with 20 mg/kg HpTx3. This dose was four-fold greater than the maximum dose (5 mg/kg) and 100-fold greater than the minimum dose (0.2 mg/kg) that were used in analgesic experiments to produce analgesic effects. The results showed that within 5 min after the injection of HpTx3 at a dose of 20 mg/kg, the mice exhibited some discomfort symptoms such as body curling and writhing; after 5 min, the symptoms became gradually weaker and disappeared completely after 10 min.

In order to detect the effect of HpTx3 on the hERG channel, we expressed the channel in HEK293T cells, followed by analysis with the whole cell patch-clamp technique. The results showed that 1 μM HpTx3 inhibited about 40% of the hERG channel current (Figure 11), suggesting that HpTx3 might have some potential cardiotoxicity. In view of the above results that even 20 mg/kg HpTx3 only caused weak and short-period adverse effects on the mice, whether the HpTx3 applied at the analgesic doses (0.2–5 mg/kg) causes adverse effects on the heart needs further investigation, and the cardiotoxicity, if indeed present, could be alleviated or eliminated by structure modification such as mutation.

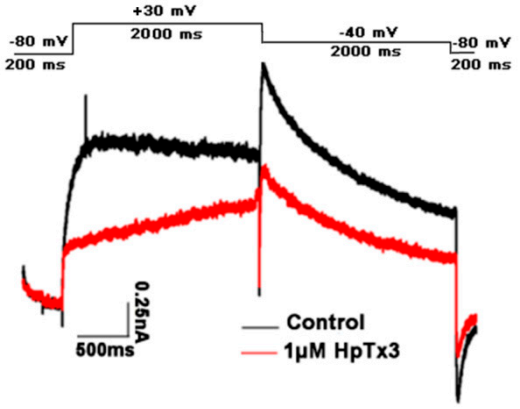


**Figure 11.** Effect of HpTx3 on the currents of the hERG channel (n = 3).

## 3. Discussion

In 1997, Sanguinetti et al. [17] isolated three new peptide toxins from the venom of the spider species *Heteropoda venatoria*, named Heteropodatoxin 1 to Heteropodatoxin 3 (HpTx1 to HpTx3). These three toxins are structurally similar and have amides on their C-termini. The conserved arrangement of the cysteine residues in HpTxs indicated that they contain an inhibitor cystine knot (ICK) motif. Electrophysiological experiments indicated that HpTxs can block $K_v4$ channels and the effects of the HpTxs, particularly HpTx 2 and HpTx3, on $K_v4.2$ channel subtype have been extensively characterized [17,23–30]. Our previous research found that the venom of *Heteropoda venatoria* has potent inhibitory effects on voltage-gated $Na^+$ channels in *Periplaneta americana* dorsal unpaired medium (DUM) neurons and rat dorsal root ganglion (DRG) neurons, indicating that the venom not only is rich in $K^+$ channel blocker neurotoxins, but also contains diverse $Na^+$ channel inhibitors [31]. These findings aroused our interest. By sequence alignment, we found that the sequence of HpTx3 has a high identity with those of some $Na_v1.7$ potential analgesic peptide toxins from the $Na_v$-targeting spider toxin family 3 (NaSpTx family 3) [7,18] (Figure 12), which suggested that HpTx3 might have an inhibitory effect on the $Na_v1.7$ channel. Our present research isolated the HpTx3 from the venom of the spider species *Heteropoda venatoria* and experimentally demonstrated that the peptide toxin has a selective inhibitory effect on the $Na_v1.7$ channel.

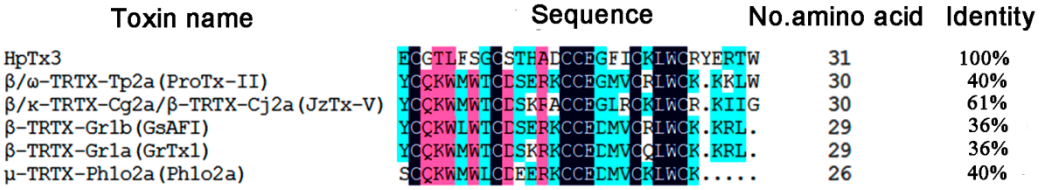


**Figure 12.** Sequence alignment of HpTx3 and some toxins in the NaSpTx family 3.

It is generally accepted that the likely promising target for therapeutic treatment to fight pain and avoid central side-effects is the neurons located in the periphery DRGs that convey pain from the skin and tendons to the central nervous system [7]. The $Na_v$ 1.7 channel subtype is considered as one of the most promising antinociceptive targets for analgesic drugs because it is abundantly present in the peripheral DRG neurons and has facilitated permeability to high molecular weight drugs [7]. $Na_v1.7$-targeting peptide toxins from spider venoms have been proposed as the candidates to replace opioids to treat pain, as the peptide toxins have advantages such as specific interaction with ion channels, easy expression, chemical synthesis, etc. [7]. Our present research found a new peptide candidate, HpTx3, which might be used to replace opioids to treat pain. HpTx3 is composed of 31 amino acids and has three disulfide bonds arranged in an inhibitor cystine knot (ICK) motif. This toxin was demonstrated to potently inhibit Nav1.7 ($IC_{50}$ 135.61 ± 12.98 nM), with at least seven-fold

selectivity over other tested $Na_v$ channel subtypes (Figure 3). It is commonly accepted that the spider toxins targeting the $Na_v1.7$ subtype with an $IC_{50}$ less than 500 nM are considered as analgesic toxin inhibitors [32]. Therefore, HpTx3 can be considered as an analgesic toxin inhibitor with high selectivity for the $Na_v1.7$.

In order to further understand the actions of HpTx3 on the $Na_v1.7$ channel, we examined the effect of the toxin on the current–voltage (I–V) relationship of the $Na_v$ channel subtype. The results indicated that HpTx3 decreased the peak current of $Na_v1.7$, but did not significantly change the initial activation voltage, the activation voltage of the maximum $Na_v1.7$ current, and the ion selectivity of the channel at depolarizing voltages ranging from –80 mV to +80 mV. When the conductance–voltage (G–V) relationship and the steady-state inactivation of $Na_v1.7$ before and after HpTx3 treatment were investigated, it was found that HpTx3 induced minor alternation in the voltage-dependence of $Na_v1.7$, shifting the activation curve to the right by 4.15 mV and the steady-state inactivation curve to the left by 7.29 mV (Figure 4C). These results suggested that the molecular mechanism of HpTx3 on $Na_v1.7$ is different from that of ProTx-II that shifts Nav1.7 channel activation in the depolarizing direction by 31.1 mV [33]. ProTx-II is a typical gating modifier toxin and can inhibit multiple sodium channel subtypes ($Na_v1.1$–$1.8$), but preferentially inhibits $hNa_v1.7$ [34]. Moreover, ProTx-II is not efficacious in rodent models of acute and inflammatory pain [35]. However, the mechanism of action of HpTx3 is somewhat similar to those of HwTx-IV [20], HnTx-III [36], HnTx-IV [37], etc.; these toxins do not alter the I-V relationship for the $Na_v1.7$ and induce minor (less than 5 mV) alterations in the voltage-dependence of its activation and steady-state inactivation [7]. Based on the mechanism of action, the $Na_v1.7$-targeting peptide toxins are classified as pore blockers and/or gating modifiers [38]. In fact, pure pore blockers or pure gating modifier toxins in nature are rare. In many cases the modes of action, namely "pore blocker" or "gating modifier", coexist with different potencies [39]. According to the action characteristics of HpTx3, we propose that this toxin acts as both a pore blocker and a gating modifier.

In order to localize the binding sites of HpTx3 on $Na_v1.7$ for further understanding the mechanism of action of HpTx3, we mutated the $Na_v1.7$ by using the domains or domain extracellular loop of $Na_v1.8$, on which 10 μM HpTx3 showed no effect (Figure 3), to replace the counterpart sequences of the $Na_v1.7$. As a result, the currents of chimeras $Na_v1.7/1.8$DIIS3b–S4 and $Na_v1.7/1.8$DIV could not be inhibited by 1 μM HpTx3 (Figure 5); the amino acid residue D816 in the DIIS3b–S4 sequence was shown to be a key residue for HpTx3 binding. It is worth mentioning that $Na_v1.6$ also has D residue in its S3b–S4 sequence. However, the inhibitory effect of HpTx3 on the $Na_v1.6$ was weaker than that on $Na_v1.7$, suggesting that there were other factors affecting the binding of HpTx3 to the ion channel. Our experimental results demonstrated that DIIS3b–S4 and DIV of $Na_v1.7$ participated in HpTx3 binding to $Na_v1.7$, and the effect of HpTx3 on $Na_v1.7$ involves the synergistic action of domain II and domain IV. We propose that the interaction of HpTx3 with DII and DIV of $Na_v1.7$ maybe at least partially contributes to the shift of the activation and steady-state inactivation curves (Figure 4), because the neurotoxins acting on Domain II of $Na_v$ channels (site 4 toxins) often affect the activation of targeted channels, and DIV-interacting (site 3) toxins affect the inactivation kinetics of the channels [40,41]. Such a cooperative action of the domain II and IV of $Na_v$ channels has also been reported previously. For example, during the interaction of RTX-VII, a toxin from the venom of the *Macrothele raveni* spider, with $Na_v1.3$, the domains II and IV of the $Na_v1.3$ cooperatively contribute to the generation of the persistent current in $Na_v1.3$ [42]. In fact, many $Na_v$-targeted toxins have been reported to have more than one binding site on $Na_v$ channels. β-scorpion toxins, for instance, like α-scorpion toxin [43,44], have additional interaction points on the extracellular domains of $Na_v$ channels in addition to their binding site on the domain IIS3–S4 extracellular loop sequence [40].

In view of the potent and selective action of HpTx3 on $Na_v1.7$, we investigated the pharmacological implications of HpTx3 in analgesia, using five different mouse pain models induced by formalin, acetic acid, hot plate, spared nerve injury, and complete Freund's adjuvant, respectively.

The formalin pain model is an effective model commonly used in pain and analgesic research [45]. In this model, formalin induces distinct biphasic nociceptive responses. The phase I responses

were thought to be produced by direct activation of nociceptive neurons by formalin, and the phase II responses were caused by the formalin-induced inflammation [21,22]. Our experimental results demonstrated that HpTx3 could efficiently inhibit the nociceptive responses in both of the two phases, suggesting that the toxin not only suppressed the pain-like behaviors induced by nociceptive nerve activation, but also inhibited those caused by inflammation induced by tissue injury. Furthermore, the effects of HpTx3 are somewhat similar to those of the centrally acting drugs that generally inhibit both of two phases equally [46]. The findings that HpTx3 and morphine, a drug that can be used as the positive control in studying central analgesic activities [47], exhibited similar analgesic effects support the conclusion. The experimental results suggest that HpTx3 can affect some central nervous system-mediated behaviors. A drug may exert such an effect after crossing the blood–brain barrier and/or by producing active components that are transported into the central nervous system [48]. However, how the HpTx3 affects the nervous system-mediated behaviors needs further investigation. Considering that HpTx3 could inhibit the pain-like behaviors caused by chemical or thermal stimuli in the mouse pain models prepared with induction of formalin, acetic acid, complete Freund's adjuvant, and hot plate, we speculate that the analgesic action of HpTx3 might involve blocking the release of prostaglandins and some other inflammation-inducing substances, because these inflammation pain models could induce pain-like behavior by releasing these bioactive components to excite nociceptive nerve endings [47].

In our present study, a sciatic nerve spared nerve injury (SNI) pain model was also developed to evaluate the analgesic effect of HpTx3. In this SNI model, the SNI-operated mice displayed rapid, strong, and persistent hypersensitivity to mechanical stimuli in the territory of the spared sural nerve, and thus are suitable to be used for detecting the mechanisms involved in mechanical pain [49]. As a result, HpTx3 was shown to display a strong analgesic effect in the SNI model, increasing the paw withdrawal threshold of the mice in a dose-dependent manner. Taken together, HpTx3 showed potent analgesic effects in all the used mouse pain models, indicating that the toxin has inhibitory action on acute, inflammatory, and neuropathic pains.

Of the nine $Na_v$ channel subtypes, $Na_v1.3$ and $Na_v$ 1.7–1.9 are widely considered to be associated with nociception and play essential roles in the pain pathway [50]. However, our experiments demonstrated that 1 μM HpTx3 has no effects on $Na_v1.3$ and even 10 μM HpTx3 does not affect the currents of $Na_v1.8$ and $Na_v1.9$. Although $Na_v1.6$ was recently reported to be associated with local inflammation and neuropathic pain [51,52], the $Na_v$ 1.6 is primarily expressed in the central nervous system and mature nodes of Ranvier in the peripheral nervous system [53], and HpTx3 preferentially inhibits $Na_v1.7$ with at least seven-fold selectivity against $Na_v1.6$. Therefore, in the HpTx3-caused analgesia, $Na_v1.7$ was the mediator and the role of $Na_v1.6$, if any, is limited. In our present study, due to the limitation of experimental conditions we did not detect the effect of HpTx3 on $Na_v1.1$. However, although $Na_v1.1$ has been demonstrated by Osteen et al. [54] to be also involved in pain, the role of the $Na_v1.1$ in the HpTx3-mediated analgesia are speculated to be relatively minor; this is because $Na_v1.1$ transcripts are primarily expressed by medium-diameter sensory neurons (only constituting 35% of all neurons within the DRG), and the $Na_v1.1$-mediated pain behaviors are not associated with neurogenic inflammation and thermal stimulation [54], whereas the $Na_v1.7$ has even extensive distribution, including being expressed in both large and small diameter DRG neurons [9], and shows efficient analgesic effects in multiple mouse pain models, including inflammation model and that induced by heat plate-produced thermal stimulation. Therefore, like $Na_v1.6$, we expect the effect of $Na_v1.1$ for HpTx3-induced analgesia to be relatively small

In addition, it should be mentioned that the HpTx3 has been demonstrated to inhibit $K_v4$ channels, particularly $K_v4.2$ [17,24,25], and the $K_v4$ channels are also involved with pain transmission. $K_v4$ channels are expressed predominately in the somata of small and large diameter nociceptors and the dorsal horn of the spinal cord, and all three $K_v4$ mRNA isoforms ($K_v4.1$–4.3) are expressed in whole DRG preparations [55–58]. Overexpression of various components of the $K_v4$ complex attenuated DGR excitability and pain phenotypes of animals [59]. The drugs that can increase A-type $K_v$ currents reverse the pain phenotype [58]. On the contrary, reduced expression of the $K_v4$ channels and knockdown of any component of the $K_v4$ channel complex in primary neurons induce

mechanical hypersensitivity, a major symptom of neuropathic pain [60,61]. Oxaliplatin, a chemotherapy drug, increases nociceptive neuron excitability to result in neuropathic pain in orofacial and other regions in patients, and the down-regulation of $K_v4.3$ channels and $I_A$ currents may be an underlying mechanism of oxalipaltin-induced orofacial neuropatic pain [62]. Peptide toxin Ts8 from the venom of the *Tityus serrulatus* (Ts) scorpion inhibited the $K_v4.2$ channel, decreasing the mechanism nociception threshold and inducing obvious nociception [63]. These observations indicate that the levels of $K_v4$ proteins and A-type currents are reversely related to the nociceptive neuron excitability. That is to say, HpTx3 inhibition of $K_v4$ channels [17,24,25] might result in hyperalgesia, an effect contrary to analgesia caused by the HpTx3 inhibition of $Na_v1.7$. Nevertheless, in our present study, HpTx3 used in several pain models showed potent analgesic activity, suggesting that the analgesic effect of HpTx3 overwhelmed the hyperalgesia it caused. This result may be explained at least partially by the fact that in the pain models the level of $K_v4$ channels is usually decreased [56,61,64,65]. Till now, only one model showed that the expression of $K_v4$ channels was increased following injury [58]. In addition, the major $K^+$ channel $\alpha$ subunit responsible for transient outward $K^+$ current ($I_{to}$) in rat is $K_v4.2$ [66], whereas the rat DRG primarily expresses $K_v4.1$ and $K_v4.3$ of $K_v4$ channels [59], which could provide an additional explanation for the cause that the analgesic effect of HpTx3 masked the hypersensitivity caused by HpTx3 inhibition of Kv4 channels. JzTx-V has similar characteristics as the toxin can inhibit $K_v$ channels including $K_v4.2$ [67], Kv4.3 [68], and $Na_v1.7$ channels [69], and it also shows a potent analgesic effect in the pain models [70].

## 4. Conclusions

The peptidic neurotoxin HpTx3 from the venom of the spider species *Heteropoda venatoria* was newly found to have a selective inhibitory action on $Na_v1.7$. With the characteristics of both pore-blocker and gate-modifier, HpTx3 does not alter the current–voltage (I–V) relationship of the $Na_v1.7$ channel but makes minor alternation in the voltage-dependence of activation and steady-state inactivation of $Na_v1.7$ by interacting with the S3b–S4 sequence in domain II and domain IV of $Na_v1.7$. During the interaction of HpTx3 with the S3b–S4 sequence of $Na_v1.7$, D816 plays a key role, whereas the E818 only plays a minor role. HpTx3 displayed a potent analgesic effect in five mouse pain models prepared based on different nociceptive mechanisms in a dose-dependent manner, suggesting that acute, inflammatory, and neuropathic pains were all attenuated by the toxin. Generally, HpTx3 at doses of ≥1 mg/kg could produce the analgesic effect comparable to that of 1 mg/kg morphine. The experimental results suggest that HpTx3 can act not only as a molecular probe in the researches on ion channel functions and pain mechanisms, but also as a lead molecule in the development of the drugs that treat $Na_v1.7$ channel-related pain.

## 5. Materials and Methods

### *5.1. Purification and Identification of HpTx3*

The venom of the spider species *Heteropoda venatoria* was collected by electrical stimulation, lyophilized and stored at –20 °C before use [71,72]. For separation, the crude venom was dissolved in distilled $H_2O$ to a final concentration of about 1 mg/mL and then subjected to semipreparative RP-HPLC (C18 column, 10 μm, 10 mm × 250 mm, Welch Materials, Inc., Shanghai, China). The loaded venom components were eluted with a linear acetonitrile gradient (20–55% acetonitrile/0.1% TFA in 45 min) at a flow rate of 3.0 mL/min. The peak containing HpTx3 [17] was collected, lyophilized, and further purified to homogeneity by analytical RP-HPLC (C18 column, 5 μm, 4.6 mm × 250 mm, Phenomenex Inc., Torrance, CA, USA). The molecular weight of the toxin was determined with an ESI mass spectrometer (6540Q-TOF, Agilent Technologies, Santa Clara, CA, USA).

### *5.2. Plasmid Construction and Transient Transfection*

All the used $Na_v$ channel subtype clones ($Na_v1.2$–$Na_v1.9$) and β subunit clones were preserved in our laboratory. cDNAs encoding rat $Na_v1.2$, rat $Na_v1.3$, human $Na_v1.5$, and mouse $Na_v1.6$ were

subcloned into the vector pcDNA3.1; cDNA encoding rat $Na_v1.4$ was subcloned into the vector pRGB4; cDNA encoding human $Na_v1.7$ was subcloned into the vector pcDNA3.1-mod; cDNAs encoding rat $Na_v1.8$ and human $Na_v1.9$ were subcloned into the vectors pCMV-HA and pEGFP-N1, respectively. For localizing the binding sites of HpTx3 on the $Na_v1.7$ and therefore probing the its mechanism of action, several chimeras were constructed with a recombination strategy by replacing the extracellular loop S3b–S4 in domain II, domain III, and domain IV of $Na_v1.7$ with the counterpart sequences of $Na_v1.8$, respectively, using the methods described [42,73,74]. As a result, three chimeras were prepared, namely, $Na_v1.7/1.8$DIIS3b–S4, $Na_v1.7/1.8$DIII, and $Na_v1.7/1.8$ DIV. Moreover, the amino acid residues D816 and E818 in the S3b–S4 sequence of $Na_v1.7$ were mutated into N ($Na_v1.7$ D816N) and Q ($Na_v1.7$ E816Q), respectively.

For heterologous expression, the vector plasmids containing wild-type (WT) $Na_v1.2$–$Na_v1.7$ and mutant plasmids were transiently transfected into HEK293T cells (China Center for Type Culture Collection, Wuhan, China) using Lipofectamine 2000 (Invitrogen, Carlsbad, CA, USA) according to the manufacturer's instructions. The vectors containing r$Na_v1.8$ and h$Na_v1.9$ were transiently transfected into the neuron-like ND7/23 cells (Spring Bioscience, Shanghai, China), which were more suitable for their heterologous expression [75,76]. In addition, the plasmids β1- and β2-eGFP, which encode the β1-subunit and β2-subunit, respectively, were co-transfected with those encoding WT $Na_v1.7$ and its mutants into the HEK293T cells. HEK293T and ND7/23 cells were maintained at 37 °C in a humidified 5% $CO_2$ incubator in Dulbecco's modified Eagle's medium (DMEM) supplemented with 10% fetal bovine serum, 2 mM L-glutamine, 100 U/mL penicillin, and 100 μg/mL streptomycin. When the cells were grown to about 90% confluence, transfection was performed with the vector plasmids. The cells with green fluorescence were selected for whole-cell patch-clamp analysis 24 h after transfection.

### *5.3. Whole-Cell Patch-Clamp Analysis*

The whole-cell patch-clamp technique was employed to analyze the effects of HpTx3 on $Na_v$ channel subtypes in the transfected HEK293T and ND7/23 cells using an EPC-10 USB patch-clamp amplifier (HEKA, Elektronik, Lambrecht, Germany). The suction pipettes with DC resistance of 2.0–3.0 MΩ were fabricated from borosilicate glass capillary tubes (VWR micropipettes; VWR Co., West Chester, PA, USA) using a two-step vertical microelectrode puller (PC-10, Narishige Co., Ltd., Tokyo, Japan). For recording the $Na^+$ currents, the suction pipettes were filled with an intracellular solution of the following composition: 140 mM CsCl, 35 mM NaCl, 105 mM CsF, 10 nM EGTA (ethylene glycol-bis (2-aminoethyl ether)-N, N, N', N'-tetraacetic acid), 10 nM HEPES (4-(2-hydroxyethyl)-1-piperazineethanesulfonic acid), pH7.4. The bath solution was composed of 140 mM NaCl, 2 mM $CaCl_2$, 1 mM $MgCl_2$, 5 mM KCl, 20 mM HEPES, and 10 mM glucose, pH 7.4. The experiments were conducted at room temperature (20–25 °C). All chemicals were products of Sigma-Aldrich (St. Louis, MO, USA) and were dissolved in sterile double-distilled $H_2O$. Data were collected with the PatchMaster software in the HEKA EPC-10 USB patch-clamp system (HEKA Elektronik, Lambrecht, Germany) and analyzed by the software Igo Pro-6.00, Prism (GraphPad Software, La Jolla, CA, USA), Sigmaplot 10.0 (Systat Software, Inc., San Jose, CA, USA), and OriginPro.

In whole-cell patch-clamp analysis, to induce ion channel currents, a 50-ms depolarization ranging from a holding potential of –80 mV to –10 mV was used for $Na_v1.2$–$Na_v1.7$, –100 mV to +20 mV, and –120 mV to –40 mV for $Na_v1.9$. When the currents of $Na_v1.8$ and $Na_v1.9$ were measured, 1 μM TTX was added to inhibit the TTX-sensitive currents. To assess the current–voltage (I–V) relationship of $Na_v1.7$, the currents were induced by a series of 50-ms step depolarization potentials ranging from –80 mV to +80 mV with a 10-mV increment at 5 s intervals. The voltage-dependence of activation was assessed with a series of test potentials in the range –80 mV to +40 mV from a holding potential of –100 mV with 10-mV increment. For detection of the voltage-dependence of inactivation, the currents were induced by a 50-ms depolarizing potential of –10 mV from various prepulse potentials for 500 ms that ranged from –120 mV to –20 mV with a 10−mV increment.

### *5.4. In Vivo Analgesic Activity Assay*

#### 5.4.1. Animals

Healthy female C57BL/6 mice (weighting 18–20 g) that were used for analgesic activity assay were obtained from the Experimental Animal Center of SLac-kinda (Changsha, China) and were randomly assigned to five groups, each group generally containing 8 mice. One group was used as the blank control, one group as the positive control treated with 1 mg/kg morphine, and three groups as the test groups treated with different concentrations of HpTx3 (0.2, 1, and 5 mg/kg), respectively. The mice were maintained at a temperature of 20–25 °C and under a 12 h light/12 h dark cycle, with free access to food and water. The ethical approval for the in vivo animal experiments was obtained from the Animal Care and Use Committee of the Hunan Province Animal Management Office. (The approval code: 219/2019).

#### 5.4.2. Formalin-Induced Paw Licking

The changes in the formalin-induced nociceptive reaction in mice was used to assess the in vivo effect of HpTx3 on $Na_v1.7$-mediated pain [74,77,78]. Paw licking, a pain-related behavior, was induced by subcutaneous intraplantar injection of formalin. The mice were intramuscularly injected into the inner thigh of the right hind limb with 100 μL 0.9% saline, morphine (1 mg/kg), or HpTx3 (0.2, 1.0, and 5.0 mg/kg), respectively, followed by subcutaneous intraplantar injection of 20 μL formalin (10%) at the right hind paw. The time that was spent to lick the injected paw by each mouse during phase I (0–10 min after injection) and phase II (15–35 min after injection) was separately recorded with a digital stopwatch. The nociceptive behavior attenuation by HpTx3 was evaluated by comparison of the paw licking times of the mice in each group.

#### 5.4.3. Acetic Acid-Induced Abdominal Writhing

Abdominal writhing responses were induced by intraperitoneal injection (i.p.) of acetic acid to C57BL/6 mice according to a previous study [10]. The mice were fasted for 12 h but were allowed to drink water freely before being used in analgesic experiments. The mice in the test groups were intraperitoneally injected with HpTx3 (0.2, 1.0, or 5.0 mg/kg) while the mice in the control groups received an equal volume of 0.9% saline. Fifteen-five minutes later, 100 μL of 1% (v/v) acetic acid were intraperitoneally injected. Then the abdominal writhing responses were observed and the writhing number of each mouse was counted for 30 min. Each bend, indent, lift, or stretch was counted as one "writhing".

#### 5.4.4. Complete Freund's Adjuvant (CFA)-Induced Hyperalgesia

According to the previously described methods with some modifications [34,78], a complete Freund's adjuvant (CFA) was administered undiluted in a volume of 20 μL by intraplantar injection at the right hind paw of four-week-old C57BL/6 mice. Paw withdrawal thresholds to mechanical stimulus in the inflamed paw were determined 24 h after the injection. HpTx3 (0.2, 1 and 5 mg/kg) and morphine (1 mg/kg) were dissolved in 0.9% saline and administered in a volume of 20 μL by intramuscular injection into the inner thigh of the right hind paw 30 min prior to the withdrawal threshold determination. The mechanical paw withdrawal thresholds were determined at 0.5, 1, 2, 3, and 4 h after the injection by using a set of calibrated Von Fery filaments with forces from 0.4 to 2.0 g (Stoelting Co., Wood Dale, IL, USA) according to the previously described method with some modifications [79]. At each time point, the plantar surface of mice was stimulated by the Von Frey filament with sufficient force to cause slight bucking against the paw, holding for up to approximately 6–8 s. The measurement was performed once every 10 s within a period of 100 s. When the number of paw withdrawal was less than 6, a next filament with increasing force was used. The smallest force (g) of the used Von Frey filaments that made the number of paw withdrawal be greater than 5 was defined as the mechanical paw withdrawal threshold at that time point.

#### *5.4.5. Hot Plate Test*

Hot plate test was conducted according to the method described [47]. The hot plate test apparatus (model YSL-21, Jinan, China) was placed in a quiet room, and the temperature was set at 55 ± 1 °C. After each mouse was placed at the hot plate, its nociceptive responses (hind-paw licking or jumping) and nociceptive threshold (paw withdrawal latency) were observed and recorded. A total of 0.9% Saline, morphine (1 mg/kg), and HpTx3 (0.2, 1, and 5 mg/kg) were separately intraperitoneally injected into the mice and the paw withdrawal latency was recorded at 0.5, 1.0, 1.5, and 2.0 h after the injection. The mice displaying abnormal baseline paw withdrawals (shorter than 5 s and longer than 30 s) were excluded from the test.

#### 5.4.6. Spared Nerve Injury (SNI)

When the SNI model was prepared, the surgery was performed according to the method of Bourquin et al. [49]. Briefly, under 1.5–2.5% isoflurane general anesthesia, the left hindlimb was fixed in a lateral position. Incision was made at mid-thigh level and a section was made through the biceps femoris in the direction of point of origin of the vascular structure to expose the three peripheral branches of the sciatic nerve. Both common peroneal and tibial nerves were ligated with a 6.0 silk thread, with the sural nerve being carefully preserved. The muscle and skin were closed in two distinct layers with the 6.0 thread. The sham surgery was performed on the control mice in the same way, without any nerve ligation. Mechanical sensitivity was recorded eighteen days after the surgery. The mice in control (sham-operated) group and test (SNI) groups each were intraperitonealy injected with 10 μL of physiological saline or HpTx3 (0.2, 1, and 5 mg/kg) in physiological saline, respectively. The plantar side of the paw ipsilateral to the surgery was stimulated with calibrated Von Frey monofilaments with forces from 0.4 to 2.0 g (Stoelting Co., Wood Dale, IL, USA) and the mechanical paw withdrawal threshold was determined as described in a complete Freund's adjuvant (CFA) model.

### *5.5. In Vivo Toxicity and the Effect of HpTx3 on the hERG Channel*

For detecting the potential in vivo toxicity of HpTx3, eight C57BL/6 mice were each intraperitoneally injected with HpTx3 at a dose of 20 mg/kg, which was 4-fold greater than the maximum dose (5 mg/kg) and 100-fold greater than the minimum dose (0.2 mg/kg) that were used in analgesic experiments.

The effect of HpTx3 on the hERG channel expressed in HEK293T cells was assayed using the whole cell patch-clamp technique according to the previous method with some modifications [80]. The bathing solution contained (in mM): HEPES 10, $MgCl_2$ 1, $CaCl_2$ 25, KCl 5, NaCl 50 (pH 7.4, adjusted with 1 M NaOH). The suction pipettes solution contained (in mM): $MgCl_2$ 2.5, KCl 140, EGTA 11, HEPES 10 (pH 7.2, adjusted with KOH). The osmotic pressure of the two solutions was adjusted to 280 ± 5 mOsm/L with sucrose. The currents of the hERG channel were induced at –40 mV after a test potential of +30 mV from a holding potential of –80 mV.

### *5.6. Data Analysis*

The acquired electrophysiological data were analyzed with SigmaPlot 10 software (Sigma, St. Louis, MO, USA) and Prism 5 (GraphPad Software, San Diego, CA, USA). Concentration–response curves were fitted by the SigmaPlot sigmoidal equation as follows: $y = a/(1 + \exp(-(x - IC_{50})/b))$, in which $IC_{50}$ is the concentration of toxin at half-maximal efficacy, and a and b are the constants. The conductance (G) at each test potential (V) was calculated according to the equation $G = I/V - V_{rev}$, where $V_{rev}$ is the reversal potential, V is the test potential, and I is the current amplitude. Normalized peak conductance was fitted with the Boltzmann equation $G/G_{max} = 1/\{1 + \exp[(V_{1/2} - V)/\kappa]\}$, where $G_{max}$ is the maximum conductance, $V_{1/2}$ is the membrane potential of half-maximal activation, and κ is the slope factor. Peak inward currents from steady-state inactivation were normalized by the maximum current amplitude and fitted with a Boltzmann equation: $I/I_{max} = 1/\{1 + \exp[(V - V_{1/2})/\kappa\}$, where V represents the inactivating prepulse potential, $V_{1/2}$ is the membrane potential of half-maximal inactivation, and κ is the slope factor.

Statistical analyses were performed using paired Student's *t*-test or ANOVA with paired comparisons. All data are presented as mean ± SD, and statistical significance was accepted at $p < 0.05$.

**Author Contributions:** Conceptualization, Xianchun Wang and Xinzhou Wu; Data curation, Xinzhou Wu, D.X. and Xianchun Wang.; Funding acquisition, Xianchun Wang; Investigation, Xinzhou Wu, Z.W., Y.C., D.X. and P.Z.; Software, Xinzhou Wu and D.X.; Supervision, Xianchun Wang; Writing – original draft, Xinzhou Wu; Writing – review & editing, Xianchun Wang.

**Funding:** This research was supported by grants from the National Natural Science Foundation of China (31870770, 31271135) and the crosswise project (53122-1371).

**Conflicts of Interest:** The authors declare no conflict of interest.

## References

1. Goldin, A.L. Resurgence of sodium channel research. *Annu. Rev. Physiol.* **2001**, *63*, 871–94.
2. Watanabe, E.; Fujikawa, A.; Matsunaga, H.; Yasoshima, Y.; Sako, N.; Yamamoto, T.; Saegusa, C.; Noda, M. $Na_v2$/NaG channel is involved in control of salt-intake behavior in the CNS. *J. Neurosci.* **2000**, *20*, 7743–7751.
3. Marban, E.; Yamagishi, T.; Tomaselli, G.F. Structure and function of voltage-gated sodium channels. *J. Physiol.* **1998**, *508 Pt 3*, 647–657.
4. Catterall, W.A. Voltage-gated sodium channels at 60: Structure, function and pathophysiology. *J. Physiol.* **2012**, *590*, 2577–2589.
5. Dib-Hajj, S.D.; Yang, Y.; Waxman, S.G. Genetics and molecular pathophysiology of $Na_v1.7$-related pain syndromes. *Adv. Genet.* **2008**, *63*, 85–110.
6. Cox, J.J.; Reimann, F.; Nicholas, A.K.; Thornton, G.; Roberts, E.; Springell, K.; Karbani, G.; Jafri, H.; Mannan, J.; Raashid, Y.; et al. An SCN9A channelopathy causes congenital inability to experience pain. *Nature* **2006**, *444*, 894–898.
7. Gonçalves, T.C.; Benoit, E.; Partiseti, M.; Servent, D. The $Na_v1.7$ channel subtype as an antinociceptive target for spider toxins in adult dorsal root ganglia neurons. *Front. Pharmacol.* **2018**, *9*, 1000–1020.
8. Blesneac, I.; Themistocleous, A.C.; Fratter, C.; Conrad, L.J.; Ramirez, J.D.; Cox, J.J.; Tesfaye, S.; Shillo, P.R.; Rice, A.S.C.; Tucker, S.J. Rare $Na_v1.7$ variants associated with painful diabetic peripheral neuropathy. *Pain* **2018**, *159*, 469–480.
9. Dib-Hajj, S.D.; Yang, Y.; Black, J.A.; Waxman, S.G. The $Na_v1.7$ sodium channel: From molecule to man. *Nat. Rev. Neurosci.* **2013**, *14*, 49–62.
10. Yang, S.; Xiao, Y.; Kang, D.; Liu, J.; Li, Y.; Undheim, E.A.; Klint, J.; Rong, M.; Lai, R.; King, G.F. Discovery of a selective $Na_v1.7$ inhibitor from centipede venom with analgesic efficacy exceeding morphine in rodent pain models. *Proc. Natl. Acad. Sci. USA* **2013**, *110*, 17534–17539.
11. Vetter, I.; Deuis, J.R.; Mueller, A.; Israel, M.R.; Starobova, H.; Zhang, A.; Rash, L.D.; Mobli, M. $Na_v1.7$ as a pain target—From gene to pharmacology. *Pharmacol. Ther.* **2017**, *172*, 73–100.
12. Savage, S.R.; Kirsh, K.L.; Passik, S.D. Challenges in using opioids to treat pain in persons with substance use disorders. *Addict. Sci. Clin. Pract.* **2008**, *4*, 4–25.
13. Hagen, N.A.; du Souich, P.; Lapointe, B.; Ong-Lam, M.; Dubuc, B.; Walde, D.; Love, R.; Ngoc, A.H. Canadian tetrodotoxin study group. Tetrodotoxin for moderate to severe cancer pain: A randomized, double blind, parallel design multicenter study. *J. Pain Symptom Manag.* **2008**, *35*, 420–429.
14. Escoubas, P.; Bosmans, F. Spider peptide toxins as leads for drug development. *Expert Opin. Drug Discov.* **2007**, *2*, 823–835.
15. Escoubas, P.; King, G.F. Venomics as a drug discovery platform. *Expert Rev. Proteomics* **2009**, *6*, 221–224.
16. King, G.F. Venoms as a platform for human drugs: Translating toxins into therapeutics. *Expert Opin. Biol. Ther.* **2011**, *11*, 1469–1484.
17. Sanguinetti, M.C.; Johnson, J.H.; Hammerland, L.G.; Kelbaugh, P.R.; Volkmann, R.A.; Saccomano, N.A.; Mueller, A.L. Heteropodatoxins: Peptides isolated from spider venom that block $K_v4.2$ potassium channels. *Mol. Pharmacol.* **1997**, *51*, 491–498.
18. Klint, J.K.; Senff, S.; Rupasinghe, D.B.; Er, S.; Herzig, V.; Nicholson, G.M.; King, G.F. Spider-venom peptides that target voltage-gated sodium channels: Pharmacological tools and potential therapeutic leads. *Toxicon* **2012**, *60*, 478–491.

19. Cestèle, S.; Qu, Y.; Rogers, J.C.; Rochat, H.; Scheuer, T.; Catterall, W.A. Voltage sensor-trapping: Enhanced activation of sodium channels by beta-scorpion toxin bound to the S3–S4 loop in domain II. *Neuron* **1998**, *21*, 919–931.
20. Xiao, Y.; Bingham, J.P.; Zhu, W.; Moczydlowski, E.; Liang, S.; Cummins, T.R. Tarantula huwentoxin-IV inhibits neuronal sodium channels by binding to receptor site 4 and trapping the domain ii voltage sensor in the closed configuration. *J. Biol. Chem.* **2008**, *283*, 27300–27313.
21. Abbott, F.V.; Franklin, K.; Westbrook, R. The formalin test: Scoring properties of the first and second phases of the pain response in rats. *Pain* **1995**, *60*, 91–102.
22. Hong, Y.; Abbott, F.V. Peripheral opioid modulation of pain and inflammation in the formalin test. *Eur. J. Pharmacol.* **1995**, *277*, 21–28.
23. Brahmajothi, M.V.; Campbell, D.L.; Rasmusson, R.; Morales, M.J.; Trimmer, J.S.; Nerbonne, J.M.; Strauss, H.C. Distinct transient outward potassium current (Ito) phenotypes and distribution of fast-inactivating potassium channel alpha subunits in ferret left ventricular myocytes. *J. Gen. Physiol.* **1999**, *113*, 581–600.
24. Kassiri, Z.; Zobel, C.; Nguyen, T.T.; Molkentin, J.D.; Backx, P.H. Reduction of I(to) causes hypertrophy in neonatal rat ventricular myocytes. *Circ. Res.* **2002**, *90*, 578–585.
25. Ramakers, G.M.; Storm, J.F. A postsynaptic transient $K^+$ current modulated by arachidonic acid regulates synaptic integration and threshold for LTP induction in hippocampal pyramidal cells. *Proc. Natl. Acad. Sci. USA* **2002**, *99*, 10144–10149.
26. DeSimone, C.V.; Lu, Y.; Bondarenko, V.E.; Morales, M.J. S3b amino acid substitutions and ancillary subunits alter the affinity of *Heteropoda venatoria* toxin 2 for $K_V4.3$. *Mol. Pharmacol.* **2009**, *76*, 125–133.
27. DeSimone, C.V.; Zarayskiy, V.V.; Bondarenko, V.E.; Morales, M.J. Heteropoda toxin 2 interaction with $K_V4.3$ and $K_V4.1$ reveals differences in gating modification. *Mol. Pharmacol.* **2011**, *80*, 345–355.
28. Wang, D.; Schreurs, B.G. Characteristics of IA currents in adult rabbit cerebellar Purkinje cells. *Brain Res.* **2006**, *1096*, 85–96.
29. Wang, Y.; Cheng, J.; Tandan, S.; Jiang, M.; McCloskey, D.T.; Hill, J.A. Transient- outward $K^+$ channel inhibition facilitates L-type $Ca^{2+}$ current in heart. *J. Cardiovasc. Electrophysiol.* **2006**, *17*, 298–304.
30. Zarayskiy, V.V.; Balasubramanian, G.; Bondarenko, V.E.; Morales, M.J. Heteropodatoxin 2 is a gating modifier toxin specific for voltage-gated $K^+$ channels of the $K_V4$ family. *Toxicon* **2005**, *45*, 431–442.
31. Huang, Y.; Wu, X.; Zhang, P.; Duan, Z.; Zhou, X.; Chen, M.; Farooq, A.; Liang, S.; Liu, Z. Peptide-rich venom from the spider *Heteropoda venator*ia potently inhibits insect voltage-gated sodium channels. *Toxicon* **2017**, *125*, 44–49.
32. Klint, J.K.; Chin, Y.K.; Mobli, M. Rational engineering defines a molecular switch that is essential for activity of spider-venom peptides against the analgesics target $Na_V1.7$. *Mol. Pharmacol.* **2015**, *88*, 1002–1010.
33. Xiao, Y.; Blumenthal, K.; Jackson, J.O.; Liang, S.; Cummins, T.R. The tarantula toxins ProTx-II and huwentoxin-IV differentially interact with human Nav1.7 voltage sensors to inhibit channel activation and inactivation. *Mol. Pharmacol.* **2010**, *78*, 1124–1134.
34. Schmalhofer, W.A.; Calhoun, J.; Burrows, R.; Bailey, T.; Kohler, M.G.; Weinglass, A.B.; Kaczorowski, G.J.; Garcia, M.L.; Koltzenburg, M.; Priest, B.T. ProTx-II, a selective inhibitor of Nav1.7 sodium channels, blocks action potential propagation in nociceptors. *Mol. Pharmacol.* **2008**, *74*, 1476–1484.
35. Priest, B.; Blumenthal, K.M.; Smith, J.J.; Warren, V.A.; Smith, M.M. ProTx-I and ProTx-II: Gating modifiers of voltage-gated sodium channels. *Toxicon* **2007**, *49*, 194–201.
36. Liu, Z.; Cai, T.; Zhu, Q.; Deng, M.; Li, J.; Zhou, X.; Zhang, F.; Li, D.; Li, J.; Liu, Y.; et al. Structure and function of hainantoxin-III, a selective antagonist of neuronal tetrodotoxin-sensitive voltage-gated sodium channels isolated from the Chinese bird spider *Ornithoctonus hainana*. *J. Biol. Chem.* **2013**, *288*, 20392–20403.
37. Cai, T.; Luo, J.; Meng, E.; Ding, J.; Liang, S.; Wang, S.; Liu, Z. Mapping the interaction site for the tarantula toxin hainantoxin-IV (β-TRTX-Hn2a) in the voltage sensor module of domain II of voltage-gated sodium channels. *Peptides* **2015**, *68*, 148–156.
38. Israel, M.R.; Tay, B.; Deuis, J.R.; Vetter, I. Sodium Channels and Venom Peptide Pharmacology. *Adv. Pharmacol.* **2017**, *79*, 67–116.
39. Redaelli, E.; Cassulini, R.R.; Silva, D.F.; Clement, H.; Schiavon, E.; Zamudio, F.Z.; Odell, G.; Arcangeli, A.; Clare, J.J.; Alagón, A.; et al. Target promiscuity and heterogeneous effects of tarantula venom peptides affecting $Na^+$ and $K^+$ ion channels. *J. Biol. Chem.* **2010**, *285*, 4130–4142.
40. Catterall, W.; Cestèle, S.; Yarov-Yarovoy, V.; Yu, F.H.; Konoki, K.; Scheuer, T. Voltage-gated ion channels and gating modifier toxins. *Toxicon* **2007**, *49*, 124–141.

41. Klint, J.K.; Smith, J.J.; Vetter, I.; Rupasinghe, D.B.; Er, S.Y.; Senff, S.; Herzig, V.; Mobli, M.; Lewis, R.J.; Bosmans, F.; et al. Seven novel modulators of the analgesic target $Na_v1.7$ uncovered using a high-throughput venom-based discovery approach. *Br. J. Pharmacol.* **2015**, *172*, 2445–2458.
42. Tang, C.; Zhou, X.; Zhang, Y.; Xiao, Z.; Hu, Z.; Zhang, C.; Huang, Y.; Chen, B.; Liu, Z.; Liang, S. Synergetic action of domain II and IV underlies persistent current generation in $Na_v1.3$ as revealed by a tarantula toxin. *Sci. Rep.* **2015**, *5*, 9241–9252.
43. Tejedor, F.J.; Catterall, W.A. Site of covalent attachment of alpha-scorpion toxin derivatives in domain I of the sodium channel alpha subunit. *Proc. Natl. Acad. Sci. USA* **1988**, *85*, 8742–8746.
44. Thomsen, W.J.; Catterall, W.A. Localization of the receptor site for alpha-scorpion toxins by antibody mapping: Implications for sodium channel topology. *Proc. Natl. Acad. Sci. USA* **1989**, *86*, 10161–10165.
45. Tjølsen, A.; Berge, O.G.; Hunskaar, S.; Rosland, J.H.; Hole, K. The formalin test: An evaluation of the method. Pain 1992, 51, 5–17.
46. Chen, Y.F.; Tsai, H.Y.; Wu, T.S. Anti-inflammatory and analgesic activities from roots of Angelica pubescens. Planta Med. 1995, 61, 2–8.
47. Meng, D.; Wang, L.; Du, J.; Chen, J.; Chen, C.; Xu, W.; Li, C. The analgesic activities of *Stauntonia brachyanthera* and YM11 through regulating inflammatory mediators and directly controlling the sodium channel prompt. *Sci. Rep.* **2017**, *7*, 7574–7586.
48. Sánchez-Navarro, M.; Giralt, E.; Teixidó, M. Blood-brain barrier peptide shuttles. *Curr. Opin. Chem. Biol.* **2017**, *38*, 134–140.
49. Bourquin, A.F.; Süveges, M.; Pertin, M.; Gilliard, N.; Sardy, S.; Davison, A.C.; Spahn, D.R.; Decosterd, I. Assessment and analysis of mechanical allodynia-like behavior induced by spared nerve injury (SNI) in the mouse. *Pain* **2006**, *122*, 14-e1.
50. Dib-Hajj, S.D.; Cummins, T.R.; Black, J.A.; Waxman, S.G. Sodium channels in normal and pathological pain. *Annu. Rev. Neurosci.* **2010**, *33*, 325–347.
51. Xie, W.; Strong, J.A.; Ye, L.; Mao, J.X.; Zhang, J.M. Knockdown of sodium channel $Na_v1.6$ blocks mechanical pain and abnormal bursting activity of afferent neurons in inflamed sensory ganglia. *Pain* **2013**, *154*, 1170–1180.
52. Xie, W.; Strong, J.A.; Zhang, J.M. Local knockdown of the $Na_v1.6$ sodium channel reduces pain behaviors, sensory neuron excitability, and sympathetic sprouting in rat models of neuropathic pain. *Neuroscience* **2015**, *291*, 317–330.
53. Habib, A.M.; Wood, J.N.; Cox, J.J. Sodium channels and pain. *Handb. Exp. Pharmacol.* **2015**, *227*, 39–56.
54. Osteen, J.D.; Herzig, V.; Gilchrist, J.; Emrick, J.J.; Zhang, C.; Wang, X.; Castro, J.; Garcia-Caraballo, S.; Grundy, L.; Rychkov, G.Y.; et al. Selective spider toxins reveal a role for the Nav1.1 channel in mechanical pain. Nature 2016, 534, 494–949.
55. Huang, H.Y.; Cheng, J.K.; Shih, Y.H.; Chen, P.H.; Wang, C.L.; Tsaur, M.L. Expression of A-type K channel alpha subunits $K_v4.2$ and $K_v4.3$ in rat spinal lamina II excitatory interneurons and colocalization with pain-modulating molecules. *Eur. J. Neurosci.* **2005**, *22*, 1149–1157.
56. Kim, D.S.; Choi, J.O.; Rim, H.D.; Cho, H.J. Downregulation of voltage-gated potassium channel alpha gene expression in dorsal root ganglia following chronic constriction injury of the rat sciatic nerve. *Brain Res. Mol. Brain Res.* **2002**, *105*, 146–152.
57. Hu, H.J.; Carrasquillo, Y.; Karim, F.; Jung, W.E.; Nerbonne, J.M.; Schwarz, T.L.; Gereau, R.W. The $k_v4.2$ potassium channel subunit is required for pain plasticity. *Neuron* **2006**, *50*, 89–100.
58. Duan, K.Z.; Xu, Q.; Zhang, X.M.; Zhao, Z.Q.; Mei, Y.A.; Zhang, Y.Q. Targeting A-type $K^+$ channels in primary sensory neurons for bone cancer pain in a rat model. *Pain* **2012**, *153*, 562–574.
59. Zemel, B.M.; Ritter, D.M.; Covarrubias, M.; Muqeem, T. A-Type KV channels in dorsal root ganglion neurons: Diversity, function, and dysfunction. *Front. Mol. Neurosci.* **2018**, *11*, 253–269.
60. Chien, L.Y.; Cheng, J.K.; Chu, D.; Cheng, C.F.; Tsaur, M.L. Reduced expression of A-type potassium channels in primary sensory neurons induces mechanical hypersensitivity. *J. Neurosci.* **2007**, *27*, 9855–9865.
61. Kuo, Y.L.; Cheng, J.K.; Hou, W.H.; Chang, Y.C.; Du, P.H.; Jian, J.J.; Rau, R.H.; Yang, J.H.; Lien, C.C.; Tsaur, M.L. $K^+$ Channel Modulatory subunits KChIP and DPP participate in $K_v4$-mediated mechanical pain control. *J. Neurosci.* **2017**, *37*, 4391–4404.
62. Viatchenko-Karpinski, V.; Ling, J.; Gu, J.G. Down-regulation of $K_v4.3$ channels and a-type $K^+$ currents in V2 trigeminal ganglion neurons of rats following oxaliplatin treatment. *Mol. Pain* **2018**, *14*, doi:10.1177/1744806917750995.

63. Pucca, M.B.; Cerni, F.A.; Cordeiro, F.A.; Peigneur, S.; Cunha, T.M.; Tytgat, J.; Arantes, E.C. Ts8 scorpion toxin inhibits the $K_v$4.2 channel and produces nociception in vivo. *Toxicon* **2016**, *119*, 244–252.
64. Conner, L.B.; Alvarez, P.; Bogen, O.; Levine, J.D. Role of $K_v$4.3 in vibration-induced muscle pain in the rat. *J. Pain* **2016**, *17*, 444–450.
65. Park, S.Y.; Choi, J.Y.; Kim, R.U.; Lee, Y.S.; Cho, H.J.; Kim, D.S. Downregulation of voltage-gated potassium channel alpha gene expression by axotomy and neurotrophins in rat dorsal root ganglia. *Mol. Cells* **2003**, *16*, 256–259.
66. Roden, D.M.; Balser, J.R.; George, A.L., Jr.; Anderson, M.E. Cardiac ion channels. *Annu. Rev. Physiol.* **2002**, *64*, 431–745.
67. Zeng, X.; Deng, M.; Lin, Y.; Yuan, C.; Pi, J.; Liang, S. Isolation and characterization of Jingzhaotoxin-V, a novel neurotoxin from the venom of the spider *Chilobrachys jingzhao. Toxicon* **2007**, *49*, 388–399.
68. Cai, L.J.; Xu, D.H.; Luo, J.; Chen, R.Z.; Chi, Y.P.; Zeng, X.Z.; Wang, X.C.; Liang, S.P. Inhibition of Jingzhaotoxin-V on $K_v$4.3 channel. *Sheng Li Xue Bao* **2010**, *62*, 255–260. (In Chinese)
69. Moyer, B.D.; Murray, J.K.; Ligutti, J.; Andrews, K.; Favreau, P.; Jordan, J.B.; Lee, J.H.; Liu, D.; Long, J.; Sham, K.; et al. Pharmacological characterization of potent and selective $Na_v$1.7 inhibitors engineered from *Chilobrachys jingzhao* tarantula venom peptide JzTx-V. *PLoS ONE* **2018**, *13*, e0196791.
70. Sun, Z.H.; Xu, D.H.; Chen, R.Z.; Cai, L.J.; Chi, Y.P.; Zeng, X.Z.; Liang, S.P. Effects of JZTX-V on mechanical allodynia in rats model with postperative pain. *J. TCM Univ. Hunan* **2009**, *29*, 27–46. (In Chinese)
71. Duan, Z.G.; Yan, X.J.; Cao, R.; Liu, Z.; Wang, X.C.; Liang, S.P. Proteomic analysis of *Latrodectus tredecimguttatus* venom for uncovering potential latrodectism-related proteins. *J. Biochem. Mol. Toxicol.* **2008**, *22*, 328–336.
72. Shu, Q.; Liang, S.P. Purification and characterization of huwentoxin-II, a neurotoxic peptide from the venom of the Chinese bird spider *Selenocosmia huwena*. *J. Pept. Res.* **1999**, *53*, 486–491.
73. Zhang, Y.; Peng, D.; Huang, B.; Yang, Q.; Zhang, Q.; Chen, M.; Rong, M.; Liu, Z. Discovery of a Novel $Na_v$1.7 Inhibitor From *Cyriopagopus albostriatus* Venom With Potent Analgesic Efficacy. *Front. Pharmacol.* **2018**, *9*, 1158–1168.
74. Zhang, Y.; Yang, Q.; Zhang, Q.; Peng, D.; Chen, M.; Liang, S.; Zhou, X.; Liu, Z. Engineering gain-of-function analogues of the spider venom peptide HNTX-I, a potent blocker of the h$Na_v$1.7 sodium channel. *Toxins* **2018**, *10*, 358–366.
75. John, V.H.; Main, M.J.; Powell, A.J.; Gladwell, Z.M.; Hick, C.; Sidhu, H.S.; Clare, J.J.; Tate, S.; Trezise, D.J. Heterologous expression and functional analysis of rat $Na_v$1.8 (SNS) voltage-gated sodium channels in the dorsal root ganglion neuroblastoma cell line ND7-23. *Neuropharmacology* **2004**, *46*, 425–438.
76. Zhou, X.; Xiao, Z.; Xu, Y.; Zhang, Y.; Tang, D.; Wu, X.; Tang, C.; Chen, M.; Shi, X.; Chen, P.; et al. Electrophysiological and pharmacological analyses of $Na_v$1.9 voltage-gated sodium channel by establishing a heterologous expression system. *Front. Pharmacol.* **2017**, *8*, 852–863.
77. Owoyele, V.B.; Adediji, J.O.; Soladoye, A.O. Anti-inflammatory activity of aqueous leaf extract of *Chromolaena odorata*. *Inflammopharmacology* **2005**, *13*, 479–484.
78. Ekberg, J.; Jayamanne, A.; Vaughan, C.W.; Aslan, S.; Thomas, L.; Mould, J.; Drinkwater, R.; Baker, M.D.; Abrahamsen, B.; Wood, J.N.; et al. μO-conotoxin MrVIB selectively blocks $Na_v$1.8 sensory neuron specific sodium channels and chronic pain behavior without motor deficits. *Proc. Natl. Acad. Sci. USA* **2006**, *103*, 17030–17035.
79. Chaplan, S.R.; Bach, F.W.; Pogrel, J.W.; Chung, J.M.; Yaksh, T.L. Quantitative assessment of tactile allodynia in the rat paw. *J. Neurosci. Methods* **1994**, *53*, 55–63.
80. Zhang, F.; Zhang, C.; Xu, X.; Zhang, Y.; Gong, X.; Yang, Z.; Zhang, H.; Tang, D.; Liang, S.; Liu, Z. *Naja atr* venom peptide reduces pain by selectively blocking the voltage-gated sodium channel Nav1.8. *J. Biol. Chem.* **2019**, *294*, 7324–7334.